ADVANCED MATERIALS
www.advmat.de

Assessing the Photovoltaic Quality of Vacuum-Thermal Evaporated Organic Semiconductor Blends

Pascal Kaienburg, Anna Jungbluth, Irfan Habib, Sameer Vajjala Kesava, Mathias Nyman, and Moritz K. Riede**

Dedicated to Professor Daoben Zhu on the Occasion of His 80th Birthday

Vacuum-thermal evaporation (VTE) is a highly relevant fabrication route for organic solar cells (OSCs), especially on an industrial scale as proven by the commercialization of organic light emitting diode-based displays. While OSC performance is reported for a range of VTE-deposited molecules, a comprehensive assessment of donor:acceptor blend properties with respect to their photovoltaic performance is scarce. Here, the organic thin films and solar cells of three select systems are fabricated and ellipsometry, external quantum efficiency with high dynamic range, as well as OTRACE are measured to quantify absorption, voltage losses, and charge carrier mobility. These parameters are key to explain OSC performance and will help to rationalize the performance of other material systems reported in literature as the authors' methodology is applicable beyond VTE systems. Furthermore, it can help to judge the prospects of new molecules in general. The authors find large differences in the measured values and find that today's VTE OSCs can reach high extinction coefficients, but only moderate mobility and voltage loss compared to their solution-processed counterparts. What needs to be improved for VTE OSCs is outlined to again catch up with their solution-processed counterparts in terms of power conversion efficiency.

1. Introduction

Organic solar cells (OSCs) have recently reached 19%[1] power conversion efficiency (PCE) and are at the brink of successful commercialization. Two fabrication technologies have been particularly successful: deposition of the photovoltaic active materials from solution, commonly applying a mixture of polymer and one or more small molecule species, and vacuum-thermal evaporation (VTE) employing only small molecules that are small enough to be successfully sublimed in vacuum. Lower equipment requirements of, for example, a spin-coater, nitrogen-filed glovebox, and a simple VTE tool for metal deposition (metal electrodes) make solution-processing more accessible to research groups compared to VTE systems requiring, sometimes elaborate and large, high vacuum chambers. However, on an industrial scale, VTE of OSCs has distinct advantages over solution processing:[2] unlike polymers, the small molecules employed in VTE can be reproducibly synthesized with defined molecular weight and purified easily.[2,3] Homogeneous layer deposition during VTE allows well-controlled thin active layers of few tens of nm, whereas upscaled solution-deposition is expected to require active layers around 200 nm[4,5] due to hard-to-control variations in the layer thickness—raising demands on the quality of charge transport in the absorber. Multilayer and multijunction stacks can be easily fabricated in VTE by sequential evaporation of layers, whereas solution processing of advanced stacks is limited by the need for orthogonal solvents, which is challenging (but not impossible) in practical terms. Last but not least, organic light emitting diodes provide precedent for VTE of successful commercial mass fabrication of organic electronics on an industrial scale which is displacing the incumbent liquid crystals in displays.

Record PCEs of solution- and VTE-processed single-junction OSCs have been roughly en par and around 10%[6–8] until 2015, with a slight advantage for polymer-based solution processing which allowed for optimized efficiencies at higher absorber thickness. These systems apply C_{60} or a solution-processable derivative as acceptor material. The dawn of efficient non-fullerene acceptors (NFAs) increased efficiencies for solution-processing to 19% as-of-today,[1] surpassing VTE PCEs which are yet to successfully employ evaporable NFAs. The challenge here is to find well-performing NFAs that are small enough so that their sublimation temperature is below their decomposition temperature. To facilitate progress in the field of VTE OSCs through molecule development, it is vital to know the strength and weaknesses of existing VTE donor molecules and blends in terms of their photovoltaic performance with C_{60}. VTE OSCs have produced record stability[9] and invaluable insights into

P. Kaienburg, A. Jungbluth, I. Habib, S. V. Kesava, M. K. Riede
Clarendon Laboratory
Department of Physics
University of Oxford
Oxford OX1 3PU, UK
E-mail: pascal.kaienburg@physics.ox.ac.uk; moritz.riede@physics.ox.ac.uk
M. Nyman
Physics, Faculty of Science and Engineering
Åbo Akademi University
Porthansgatan 3, Turku 20500, Finland
The ORCID identification number(s) for the author(s) of this article can be found under https://doi.org/10.1002/adma.202107584.

DOI: 10.1002/adma.202107584

the physics of OSCs,[10] especially regarding the influence of the charge-transfer (CT) state on device operation. However, comprehensive, and comparative characterization of absorber blends, combining photo-physical and transport measurements, are scarce for VTE OSCs.

Here, we carry out comprehensive characterization of three select donor:C_{60} VTE systems and quantify the most important material properties that govern photovoltaic performance. Based on a meta-analysis of literature reports on VTE OSC, we select ZnPc:C_{60}, F_4ZnPc:C_{60}, and DCV5T-Me(3,3):C_{60} (short DCV5T-Me:C_{60} in the following) for showing qualitatively different behavior in term of their *J*–*V* performance. Our in-depth characterization finds that these systems indeed span a wide range of values in terms of optical band gap, maximum extinction coefficient, voltage loss, and mobility. These systems thus provide a representative sample of the performance space that VTE OSCs cover today. We also investigate DTDCPB:C_{60} and HB194:C_{60} to extend the number of investigated donor molecules and demonstrate the viability of our methodology. Since the values we obtain for these two blends fall into the range of those found for the first three material systems we will focus our discussion on these three. Based on our selected sample of molecules, understanding how molecular properties impact blend characteristics and affect device performance will support the rational design of novel molecules with increased performance. In the future, it is desirable to combine the favorable properties of different molecules identified in this study, in one molecule, which would significantly enhance photovoltaic performance.

2. Vacuum Thermal-Evaporated Solar Cells

To select material systems for this study, we carried out a meta-analysis of VTE OSC performance reported in literature. The summary is shown in **Figure 1**a. In our analysis we assess the photovoltaic quality of material blends by considering how well the absorption edge matches the AM1.5g sun spectrum, the voltage loss at open circuit under standard reporting conditions, and the charge carrier collection efficiency. The first two are reflected in η_{Sch} in an adaptation of Scharber's efficiency prediction[11] but instead of looking at the HOMO level offset of donor and acceptor molecules, we directly consider the voltage loss between the optical band gap and open-circuit voltages (V_{oc}). For the optical band gap, we use the inflection point of the low-energy tail of the external quantum efficiency (EQE) as reference energy, for example, in a way that is relevant for photovoltaic devices.[12,13] Since η_{Sch} assumes a constant fill factor (FF), it neglects variations of charge carrier collection efficiency. This important aspect of OSC performance is captured by the electronic quality factor[13] $Q = \mu^2/\beta^{0.8}$, where μ is the mobility and β the bimolecular recombination coefficient, on the *y*-axis in Figure 1a. Q is calculated from the FF after deconvoluting effects from the device stack, in particular the absorber layer thickness, resulting in a blend-specific and device-independent quantity, which reflects the competition between transport and recombination in the solar cell. Both figures of merit are calculated for a range of high-performing or notable blends[14–23] reported in literature, and plotted in Figure 1a, with material systems and values listed in Table S1, Supporting Information. The efficiency is coded in color and symbol size and it is evident that higher Q and higher η_{Sch} produce higher efficiencies for optimized device stacks.

To put the values in Figure 1a into context,[24] the best VTE OSCs reach better energy level matching in this analysis than historic record-performing polymer:PCBM systems, where $\eta_{Sch} \lesssim 10\%$, but lag behind more recent NFA-based systems reaching up to $\eta_{Sch} = 16\%$. With $Q \lesssim 1$ cm$^{1.6}$ V^{-2} s$^{1.2}$, the electronic quality of VTE OSCs is distinctly lower than

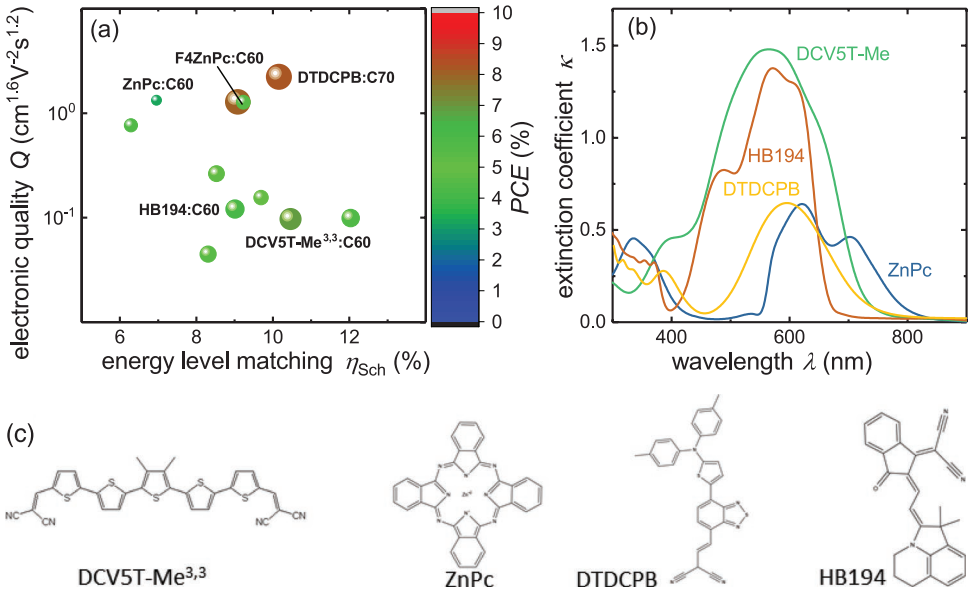

Figure 1. a) Meta-analysis of noticeable and well-performing VTE OSCs reported in literature according to refs. [13,24]. The experimental PCE is color- and size-coded. The energy level matching reflects the matching of absorption edge and AM1.5g solar spectrum, as well as voltage losses. The device-independent electronic quality governs a material blend's ability to efficiently collect photogenerated charges. Figure S8, Supporting Information, shows a corresponding analysis for solution-processed polymer-based systems for reference. b) Extinction coefficient (in-plane) of strong-absorbing DCV5T-Me and HB194 and weak-absorbing ZnPc and DTDCPB. F_4ZnPc closely matches κ of ZnPc. c) Molecular structures of investigated donor molecules.

that of polymer:PCBM systems reaching Qs between 10 and 10^4 $cm^{1.6}$ V^{-2} $s^{1.2}$ (polymer:NFA blends reach roughly an order of magnitude lower Q than their fullerene counterparts). As a side note, the lower Q explains why optimal thicknesses of NFA systems are at the moment typically limited to 100 nm, while certain polymers perform best at 200–300 nm with PCBM.

Our selection of experimentally investigated material systems in this study directly follows from Figure 1a: ZnPc:C_{60} shows one of the highest Q while performing poorly in terms of η_{Sch}. On the other hand, DCV5T-Me:C_{60} has an excellent η_{Sch} and is one of the best performing VTE systems, but has an order of magnitude lower Q. These two blend systems thus reflect different extremes of a wide range of VTE donor:C_{60} systems. In addition, we examine F_4ZnPc:C_{60} as an intermediate system, since it shows improved η_{Sch} compared to ZnPc:C_{60} while maintaining the relatively good Q of ZnPc:C_{60} blends. To further verify our methodology and include additional donor molecules, we study the high-performing blend DTDCPB:C_{60}[18] as well as the merocyanine dye HB194:C_{60}[20] which shows an intermediate Q. The molecular structures are shown in Figure 1c. The merit of this meta-analysis in terms of Q and η_{Sch} is that it provides a 0th order assessment of the photovoltaic potential of molecule blends from basic device characterization, namely J–V, EQE, and absorber thickness. However, the assessment is somewhat crude as it does not clarify the origin of voltage losses and does not deconvolute mobility and recombination. More specific insights—invaluable, for example, for the rational design of new molecules—require more sophisticated analysis and advanced optoelectronic characterization and analysis as presented later in this manuscript.

To complete our initial assessment of material properties essential to OSC performance, we consider the extinction coefficient[25] of ZnPc and DCV5T-Me in Figure 1b. The larger optical band gap, resulting from a higher energy of the lowest-lying singlet S1, of DCV5T-Me compared to ZnPc is unfavorable for PV performance but already accounted for in the figure of merit η_{Sch}. HB194 and DTDCPB also classify as high optical-gap absorber. Apart from the spectral shape, the strength of absorption directly affects the PV performance potential of a material,[25,26] and strong absorption is cited as one of the reasons for high performance of NFAs.[27] Figure 1b shows the in-plane extinction coefficient relevant for absorption under normal incidence. The out-of-plane component is shown in Figure S8, Supporting Information. The peak extinction coefficient of DCV5T-Me is more than double that of ZnPc and comparable to values of NFAs, which is maybe unsurprising since DCV5T-Me shares the A–D–A structure of high efficiency NFAs. The dye HB194 shows similarly high maximum extinction. The weak absorption of ZnPc and F_4ZnPc, even compared to many polymers peaking at $\kappa = 1$,[26] contributes to their relatively poor performance in terms of PCE. DTDCPB reaches high efficiency in literature reports[18] but Figure 1b clearly demonstrates that its weak absorption is a drawback for OSC performance.

3. Device Performance

The voltage losses at open circuit (under standard reporting conditions) as well as transport and recombination dynamics presented in this work were carried out on full solar cells, meaning that all findings are directly device relevant. Solar cells were fabricated in vacuum via subsequent thermal evaporation of MoOx (3 nm)/donor:C_{60} (varied)/BPhen (8 nm)/Al (≈100 nm) on top of an ITO-coated glass substrate held at room temperature. The donor:C_{60} absorber blends were co-evaporated in a 2:1 molar ratio, except DTDCPB:C_{60} and HB194:C_{60} to match literature reports[18,20] as described in the Experimental Section. The corresponding current density–voltage (J–V) characteristics are shown in **Figure 2** for the donor:C_{60} blends based on ZnPc, F_4ZnPc, and DCV5T-Me, with the other two blends shown in Figure S1, Supporting Information, for better overview. Figure 2a displays devices with $d = 50$ nm thick absorber layer and Figure 2b displays absorber layers of about 100 nm. The spectral mismatch-corrected[28] performance for all devices is listed in **Table 1** and dark J–Vs and EQEs can be found in Figures S1 and S2, Supporting Information, respectively. The V_{oc} of all devices changes little with thickness and correspond closely to the literature records used in Figure 1 (see Table S1, Supporting Information). The FF of all systems

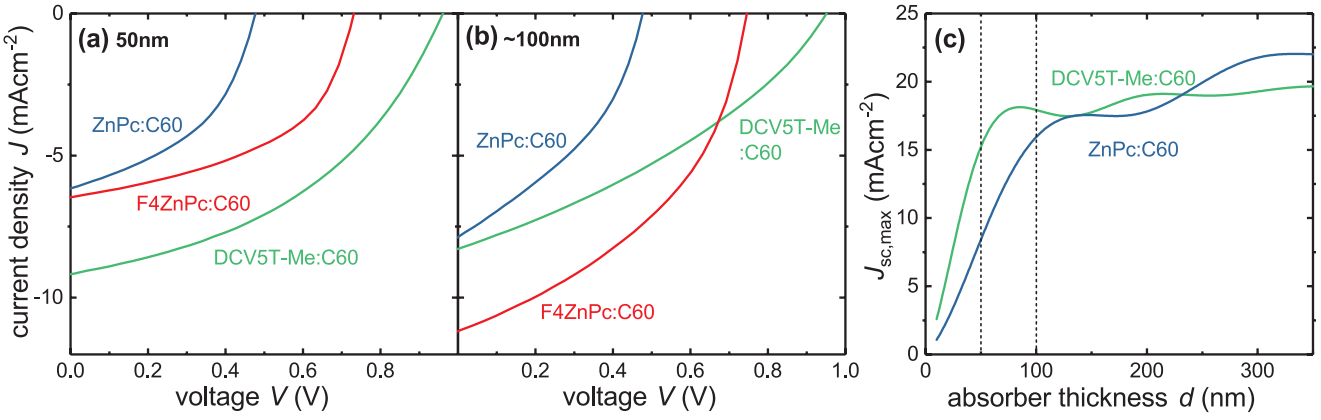

Figure 2. Current density–voltage (J–V) characteristic of the three select material systems used to determine photovoltaic performance for a) 50 nm, and b) 100 nm (ZnPc:C_{60}, F_4ZnPc:C_{60}), and 110 nm (DCV5T-Me:C_{60}) absorber thickness d. Voltage losses are later quantified for the 50 nm devices and mobility for the 100 nm devices. c) Optical TMM simulations to illustrate the difference thickness dependence of the ideal maximum short circuit density $J_{sc,max}$ (assuming EQE = 1) of DCV5T-Me:C_{60} and ZnPc:C_{60}.

Table 1. Mismatch-corrected solar cell performance under AM1.5g illumination for data shown in Figure 2 and Figure S1, Supporting Information.

Blend	d [nm]	V_{oc} [V]	FF [%]	J_{sc} [mA cm^{-2}]	PCE [%]
DCV5T-Me:C_{60}	50	0.961	43	10.0	4.1
	110	0.951	34	9.0	2.9
ZnPc:C_{60}	50	0.477	45	5.9	1.3
	100	0.477	38	7.4	1.3
F_4ZnPc:C_{60}	50	0.732	49	6.3	2.3
	100	0.746	43	10.5	3.4
DTDCPB:C_{60}	50	0.942	54	7.5	3.8
	135	0.899	37	6.3	2.1
HB194:C_{60}	50	0.939	45	9.6	4.1
	100	0.914	33	7.3	2.2

drops with thickness, as expected for fully depleted absorber layers where charge carrier collection strongly depends on voltage.[13,29,30]

The behavior of the short-circuit current density J_{sc} differs for the three systems when going from 50 to 100 nm absorber thickness in Figures 2a and 2b, respectively. J_{sc} increases for ZnPc:C_{60} and, is more pronounced, F_4ZnPc:C_{60} while it decreases for DCV5T-Me:C_{60}, DTDCPB:C_{60}, and HB194:C_{60}. For efficient exciton separation, the J_{sc} is governed by the absorptance of the absorber layer and the charge collection efficiency. Even for 50 nm thickness, and more pronounced for ≈100 nm, all systems suffer from imperfect charge collection at J_{sc}, as can be seen from the unsaturated current density in Figure 2a,b and Figure S1, Supporting Information. Note that the devices do not suffer from strong shunting as can be seen from the dark J–V in Figure S1, Supporting Information, so that the voltage dependence of illuminated J–V curves around $V = 0$ V can indeed be attributed to charge collection issues.

To explain an increase in J_{sc} with thickness, the losses in charge collection efficiency must be compensated by a larger increase in absorptance at higher thickness. Figure 2c compares optical transfer matrix method (TMM) simulations of ZnPc:C_{60} and DCV5T-Me:C_{60}. It shows the ideal J_{sc} that would be obtained if all photogenerated carriers were collected, that is, internal quantum efficiency (IQE) = 1 for all wavelengths, and thus holds similar information as the absorptance. The simulations qualitatively illustrate that for the strongly absorbing DCV5T-Me-based blend absorption at 50 nm is already quite high while the weaker-absorbing ZnPc-based blend shows much larger gains for a thicker absorber. Similarly, significant gains would be made for ZnPc blends when going from the first ($d \approx 150$ nm) to the second interference maximum ($d \approx 300$ nm) while gains are almost marginal for DCV5T-Me:C_{60}. Note that an optical spacer layer between active layer and the back electrode would increase absorption in the absorber layer for low thickness as demonstrated in Figure S3, Supporting Information. Unlike with solution-based processing, optical spacer layers can be easily fabricated with VTE and are commonly applied in optimized VTE OSC,[31] allowing for decent absorptance even at the typical low absorber thickness between 30 and 70 nm.

In summary, an increased absorptance at 100 nm compared to 50 nm absorber thickness, seems to compensate charge carrier collection losses at J_{sc} for the ZnPc and F_4ZnPc systems, which is not the case for DCV5T-Me:C_{60}. The fact that no optical spacer is applied, and that the absorber thickness is kept comparable rather than individually optimized in this study explains the overall lower values for J_{sc} and FF, and consequently PCE, when comparing to optimized stack performance in literature.[14,15,32] We cannot exclude that fine-tuning of other processing parameters, such as the temperature of the substrate during deposition or the donor–acceptor blend ratio, in the cited literature leads, for example, to a somewhat better morphology. However, the fact that V_{oc} is very comparable to literature indicates that the investigated samples and the extracted values discussed later in this article are meaningful and representative for the material systems under consideration. To further support this claim, we calculate Q and η_{Sch} from the J–V characteristics of our samples and find values that match literature well (see Table S1, Supporting Information).

4. Voltage Losses

We employ sensitive EQE measurements with large dynamic range shown in **Figure 3**a to assess voltage losses and estimate CT state properties with Marcus theory. Compared to F_4ZnPc:C_{60}, the ZnPc:C_{60} spectrum has a clear shoulder in the subgap region indicating a larger energetic difference between CT state and ZnPc's lowest lying singlet S1. Note that the leveling off at the spectrum at low signals is caused by the noise floor, that is, the detection limit of our setup at about 5×10^{-7}. Gaussian fits of the absorption tail shown in Figure S4, Supporting Information, yield CT state energies of 1.19 and 1.47 eV for ZnPc:C_{60} and F_4ZnPc:C_{60}, respectively, which closely matches values reported in literature.[10] The DCV5T-Me:C_{60} spectrum is shifted to higher energies due to its larger optical band gap and has a similarly feature-free absorption tail as F_4ZnPc:C_{60}. To obtain a good fit for DCV5T-Me:C_{60}, the S1 and CT peak are fitted subsequently[33,34] and $E_{CT} = 1.51$ eV is obtained, which is comparable to literature reports.[10,35] The EQE data for DTDCPB:C_{60} and HB194:C_{60} is shown in Figure S4, Supporting Information, for better clarity of the graphic. A slight shoulder is discernible for HB194:C_{60} while the CT state of DTDCPB:C_{60} is not clearly visible.

In Figure 3b, we split the voltage losses in our solar cells according to detailed balance theory, assuming reciprocity between absorption and emission[10,36,37] and closely following the method in refs. [24,12]. The values can be found in Table S3, Supporting Information. From the optical band gap, we calculate the theoretical maximum V_{oc}^{SQ} in the radiative limit.[38] From there we split the difference between V_{oc}^{SQ} and the measured V_{oc} into losses from short-circuit currents below the theoretical maximum ΔV_{oc}^{sc}, as well as radiative ΔV_{oc}^{rad} and nonradiative contributions ΔV_{oc}^{nr}. To obtain accurate values of the radiative open-circuit voltage V_{oc}^{rad}, we extend the experimental data by the CT state fits shown in Figure S4, Supporting Information, yielding saturated V_{oc}^{rad} as shown in Figure S5, Supporting Information.

As can be seen from Figure 3c, DCV5T-Me:C_{60}, DTDCPB:C_{60}, HB194:C_{60}, and F_4ZnPc:C_{60} show similar values

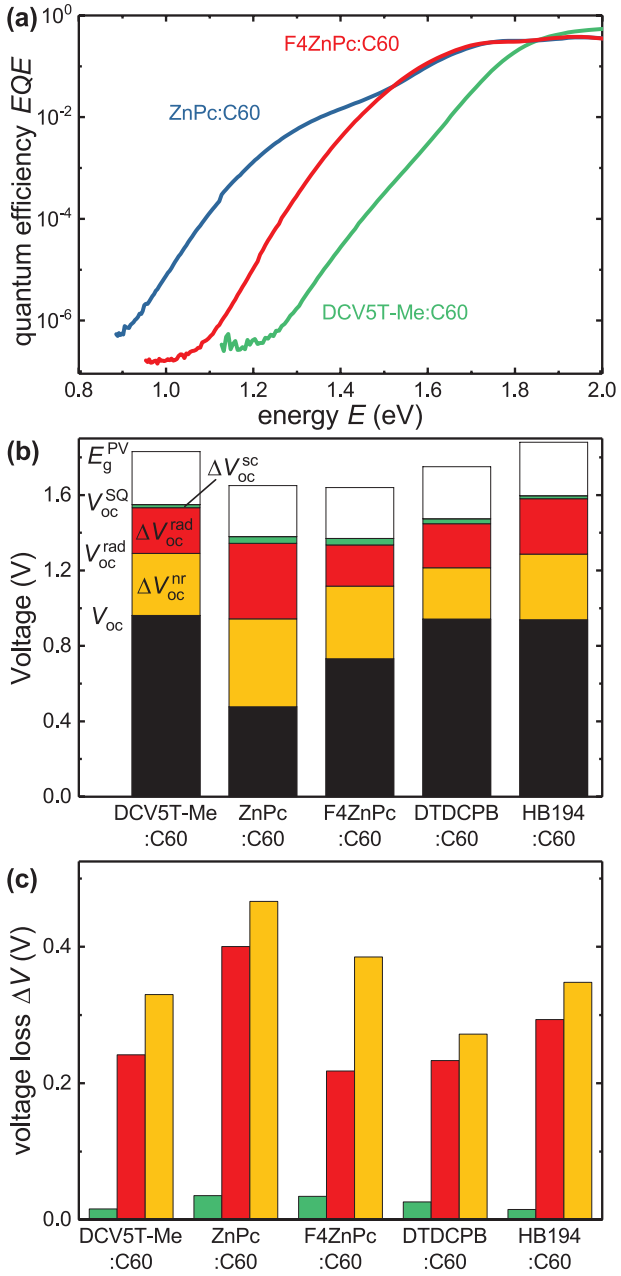

Figure 3. a) Sensitive EQE measurements of the select systems for 50 nm absorber thickness, with ZnPc:C_{60} being the only material showing a discernible shoulder in the subgap region. See Figure S4, Supporting Information, for DTDCPB:C_{60} and HB194:C_{60} data. b) Dissection of V_{oc} following ref. [12] for all five investigated material systems based on the data shown in (a) and Figure S4, Supporting Information. c) Loss terms shown in (b) displayed individually. The low CT energy of ZnPc:C_{60} causes enhanced radiative losses. Nonradiative losses dominate and are in qualitative agreement with the energy gap law.[10]

for the different voltage loss terms, while those of ZnPc:C_{60} are significantly higher. The voltage loss ΔV_{oc}^{sc} is small compared to radiative and nonradiative losses as is typically the case for OSCs[39,40] even if measured J_{sc} values are well below the theoretical maximum. Radiative losses are slightly above 200 meV for DCV5T-Me:C_{60}, DTDCPB:C_{60}, and F_4ZnPc:C_{60}, and almost twice as high for ZnPc:C_{60}, with HB194:C_{60} ranking in between. DCV5T-Me:C_{60}, F_4ZnPc:C_{60}, and ZnPc:C_{60} are in range of literature reports on these material systems,[10,35] while, we are not aware of reported loss analysis on the other two systems. Notably, the radiative losses in DCV5T-Me:C_{60}, DTDCPB:C_{60}, and F_4ZnPc:C_{60} are below those of PTB7:PCBM,[41] one of the best-performing polymer:fullerene systems in terms of energy level matching η_{Sch}.[24] However, many NFA-based blends yield much lower radiative losses down to few tens of meV.[41] Such systems are often referred to as low-offset systems in reference to the small energetic difference between the energy of the lowest lying singlet and the CT state energy. It should be kept in mind though that comparing radiative losses across literature requires a consistent definition of the optical band gap, which is yet to be agreed on.[40] Since the report cited on PTB7 and NFAs applies the same definition via the EQE inflection point, the values discussed here can indeed be compared.

Nonradiative losses are the largest source of voltage losses at open circuit in all five systems, with DTDCPB:C_{60} showing the lowest loss values. The trend that nonradiative losses are largest for ZnPc:C_{60}, followed by F_4ZnPc:C_{60}, and DCV5T-Me:C_{60} is in qualitative agreement with the energy gap law for nonradiative recombination which states that nonradiative losses scale inversely with the CT state energy[10]—and thus V_{oc}^{rad}. The nonradiative losses we obtained for our five material systems lie well within the bounds of other fullerene-based systems but distinctively above (many) NFA-based systems when locating the data in recently published scatter plots of assembled datasets from literature of ΔV_{oc}^{nr} versus E_{CT}[42] or V_{oc}.[27]

5. Mobility and Recombination

We now turn to the blends' ability to efficiently extract photogenerated charges. The decisive material parameters here are the mobility μ and the recombination coefficient β assuming a bimolecular recombination rate $R = dn/dt = \beta np$, with equal (total) electron and hole charge carrier densities $n = p$ for undoped devices. The transport and recombination (at V_{oc}) yielding μ and β can be probed in a single experiment of OTRACE.[43] This CELIV[44]-variant, unlike often used field-effect transistor measurements, provides solar cell relevant mobilities that are more robust than commonly applied space-charge-limited current (SCLC) measurements.[45,46] To reduce the influence of the RC constant, we measured the ≈100 nm thick samples which have longer transit and t_{max} times than the thin samples. In our OTRACE measurements, the solar cell is illuminated with a light pulse long enough to reach a stable V_{oc}, in this case 100 µs. Then, the light is switched off and the device is kept at open circuit for a defined delay time during which some of the charge carriers recombine and the V_{oc} decays accordingly. Then, a linearly increasing voltage pulse toward low and eventually negative voltages is applied to sweep out all photogenerated carriers remaining after the delay.

The extraction current during the voltage pulse is shown in **Figure 4**a for the example of DCV5T-Me:C_{60} with different traces corresponding to different delay times. The traces for all other systems are shown in Figure S6, Supporting

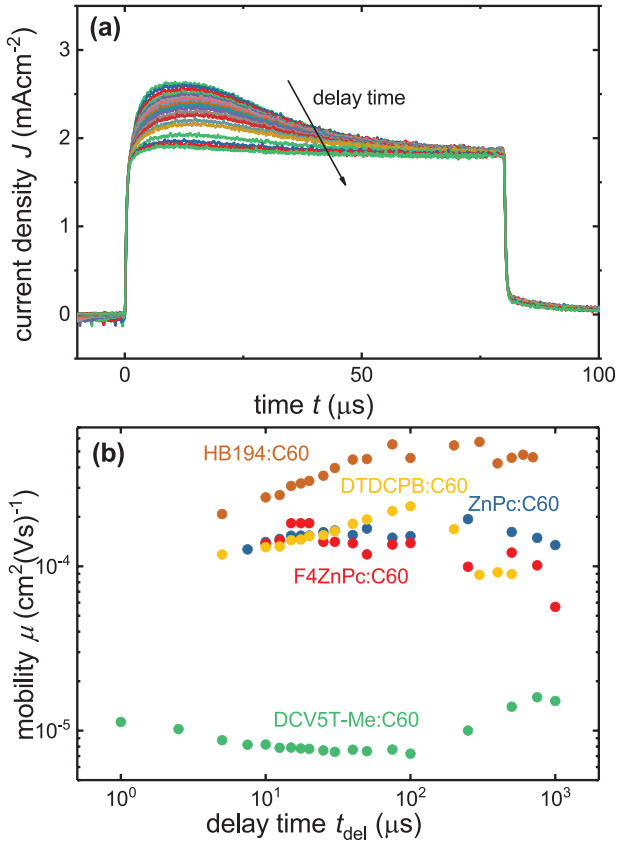

Figure 4. a) OTRACE signals for 100 nm DCV5T-Me:C_{60}. Different traces correspond to different delay times. RC effects are negligible since $t_{max} \gg RC$. b) Resulting mobility values with DCV5T-Me showing an order of magnitude lower μ than ZnPc:C_{60} and F_4ZnPc:C_{60}.

Information. For the mobility, the time, t_{max}, at which the current peaks is extracted and analyzed according to theory developed for photo-CELIV.[47,48] We apply the formula proposed by Lorrmann et al.[49] which is a better approximation for a wide range of current peak heights including those observed in our experiments. Note that this—and other—models do not include space-charge effects or trapping of charge carriers. The calculated values for mobility versus delay time are shown in Figure 4b. The t_{max} is determined for the current with the largest value rather than manually estimating the peak maximum. For this reproducible approach free from human bias, noise in the traces will translate into some noise in the t_{max} and μ, even after smoothening (with a Savitzky–Golay filter) of the data, which explains the jitter in μ. For long delay times and low charge carrier densities, locating the peak position becomes difficult. Most importantly, ZnPc:C_{60} and F_4ZnPc:C_{60} show a similar mobility of $\mu \approx 1.6 \times 10^{-4}$ cm^2 V^{-1} s^{-1} and $\mu \approx 1.2 \times 10^{-4}$ cm^2 V^{-1} s^{-1}, respectively. DTDCPB:C_{60} shows a comparable mobility of $\mu \approx 2.0 \times 10^{-4}$ cm^2 V^{-1} s^{-1}. These values are one order of magnitude higher than that of DCV5T-Me:C_{60}. The low $\mu \approx 0.8 \times 10^{-5}$ cm^2 V^{-1} s^{-1} of the latter can explain the low Q and FF discussed at the beginning of this paper, as well as the low optimized thickness of 30 nm in ref. [14]. Mobilities in polymer-based solution-processed solar cells typically reach values above 10^{-4} cm^2 V^{-1} s^{-1} for optimized morphologies.[4]

While the four previously discussed systems show consistency between measured values for mobility and device performance parameters, HB194:C_{60} seems to be an exception. Its measured mobility is comparably high and one would expect a higher Q and FF, as well as higher optimized thickness in literature report.[20] A potential reason for the high value measured could be an imbalance between electron and hole mobilities. In OTRACE measurements, the faster carrier species will dominate the signal. Optimizing blend ratios with respect to device performance typically yields roughly balanced mobilities, which cannot be guaranteed for the fabricated devices. Separate measurement of electron and hole mobilities, for example, through MIS-CELIV measurements,[50] would be required to provide clarification, which is beyond the scope of this study.

By integrating the extraction peak, the number of (mobile) charge carriers n in the device is obtained. The derivative then yields the recombination rate R, which is plotted against n^2 in Figure S7, Supporting Information, for all material systems. For purely bimolecular recombination, a straight line is expected, which is not the case over the measured range. In fact, a log–log plot in Figure S7, Supporting Information, indicates clear deviations from slope 2. When fitting the higher density regime, a value for β can be extracted, which is given in Figure S7, Supporting Information. However, these values should be treated with care for the discussed deviation from second-order recombination. Reasons for such deviation include competing recombination mechanisms (during the delay) such as trap-assisted Shockley–Read–Hall as well as surface recombination. Furthermore, it has been shown for other techniques probing recombination, such as transient photovoltage and transient photocurrent, that inhomogeneous carrier profiles and carrier trapping may cause apparent deviations from a second-order process, even if the dominating microscopic recombination process is in fact of bimolecular nature, for reasons related to the device structure and experimental conditions.[51–53]

6. Classification of Material Systems

We will now tie in the results of our previous analysis to obtain a classification of the investigated material systems according to the four quantities extinction coefficient, optical band gap, radiative losses, and mobility. The cumulative behavior in these four categories determines the photovoltaic efficiency potential of a specific blend of organic molecules. **Table 2** shows the results of this characterization for our five selected material systems. The proposed classification is not limited to VTE systems but equally applies to solution-processed OSC blends. In fact, the grouping into "high," "moderate," and "low" is primed by what is achieved for solution-processed OSCs in each category. We added one example of a solution-processed system with indicated references for comparison and a wider adoption of reporting these parameters would help the comparability and classification of OSC in general.

In our methodology we argue that, in a first order approximation, the radiative losses ΔV_{oc}^{rad} are the crucial quantity when assessing voltage losses. This is because radiative losses largely govern nonradiative ones and there are two regimes: Whenever the energy gap law is valid, as seems to be the case for

Table 2. Classification of the five investigated VTE material blends according to the key photovoltaic properties of OSCs assessed in this work. Additional literature data from solution-processed polymer-based OSC is given for reference. For consistency, ΔV_{oc}^{rad} is calculated by taking V_{oc}^{rad} from the reported value and taking E_g as defined in this work via the EQE inflection point.

Blend	Extinction [κ]	Optical band gap [E_g] [eV]	Radiative loss [ΔV_{oc}^{rad}] [V]	Mobility [μ] [cm^2 V^{-1} s^{-1}]
DCV5T-Me:C_{60}	1.5 High $\gg$ 1	1.83 High $\gg$ 1.5 eV	0.24 Moderate $\approx$ 0.2	0.8×10^{-5} Low $\ll 10^{-4}$
ZnPc:C_{60}	0.63 Low $\ll$ 1	1.65 Moderate $\approx$ 1.5	0.4 High $\gg$ 0.2	1.6×10^{-4} Moderate $\approx 10^{-4}$
F_4ZnPc:C_{60}	$\approx$ as ZnPc	$\approx$ as ZnPc	$\approx$ as DCV5T-Me	$\approx$ as ZnPc
DTDCPB:C_{60}	0.65 Low	1.75 Mod.-high	0.23 Moderate	2.0×10^{-4} Moderate
HB194:C_{60}	1.4 High	1.88 High	0.29 Mod.-high	5.0×10^{-4} Moderate
PTB7:PCBM	$\approx$0.75[26] Mod.-low	$\approx$1.7[41] Mod.-high	$\approx$0.25[41] Moderate	
PCDTBT:PC_{71}BM	$\approx$0.95[26] moderate	1.94[54] high	0.4[39] high	4.0×10^{-5}[43] Low (OTRACE)
PM6:Y6	Y6: 1.5 high PM6: 1 mod[55]	1.41[42] Low-mod.	0.05[42] low	2.0×10^{-4}[5] Moderate (i-TOF)

most fullerene-based systems, nonradiative losses are given by E_{CT} and thus $V_{oc}^{rad} = E_{opt} - \Delta V_{oc}^{rad}$. When very small ΔV_{oc}^{rad} are achieved, for example, in certain NFA-based blends mentioned above, the energy gap law does not apply anymore,[42] and hybridization[42,55–57] of singlet and CT state causes nonradiative voltage losses to be capped and roughly constant.[42]

For any combination of donor and acceptor, the radiative losses are a consequence of the CT state formed by the donor and acceptor molecules, and these losses will differ if one of the molecular species is varied. The extinction coefficient and optical band gap, on the other hand, are characteristic of an individual molecular species and change very little by being blended with another molecular species. And while ultimately the extinction coefficient of the material blend, which will depend on the blend ratio, governs the absorptance, the solar cell will benefit from high extinction of either species. It makes thus sense to assess extinction coefficient of donor and acceptor molecule separately. For VTE OSC, where all well-performing blends apply C_{60} as acceptor as-of-today, the four categories refer directly to the donor molecule or the properties of the donor molecule in combination with C_{60}. It can be expected that, for example, radiative losses for ZnPc would be moderate or low when combined with a suitable NFA.

While the first three categories are fairly robust for a given molecule species or donor:acceptor combination, the case for the mobility in the blend is more sophisticated since transport properties depend on morphology and thus deposition conditions. However, for reasonably well-optimized systems, the mobility of the blend will be close to its optimum value as well. Based on this, we deem it unlikely that, for example, DCV5T-Me:C_{60} will achieve moderate or high mobilities. Indeed, fine-tuning of deposition conditions[32] improved performance of DCV5T-Me:C_{60}, but the optimum thickness increased merely from 30[14] to 40 nm.[32] This indicates that improvements in mobility, achieved by highly optimizing typical fabrication parameters, are important to reach highest OSC performance, they are nevertheless only incremental. One exception to this notion is if new processing parameters are found that fundamentally alter the deposition kinetics.[58] Finally, when comparing the mobilities of different systems it is important that 1) the same characterization method is applied for all systems since different techniques yield different values for the mobility,[59] and 2) the applied method is reliable. Here, photo-CELIV[47,48] or OTRACE[43] are good candidates, whereas, for example, SCLC measurements are prone to errors.[45,46]

7. Conclusion

We presented a comprehensive assessment of photovoltaic material quality for three material systems whose properties reflect the breadth of VTE OSCs. These example systems cover significant variation in extinction coefficient, optical band gap, radiative losses (and thus nonradiative losses according to the energy gap law), as well as mobility. Judging the investigated material blends in relation to polymer-based solution-processed OSCs, comprising fullerenes and NFAs, ZnPc:C_{60} can be classified along the four quantities analyzed as low-extinction, moderate band gap, large-radiative loss, and moderate-mobility system. F_4ZnPc:C_{60} falls into the same categories, except having moderate radiative loss. Finally, DCV5T-Me:C_{60} is a high-extinction, large band gap, moderate radiative loss, and low-mobility system. The performance of DTDCPB:C_{60} and HB194:C_{60} varies across the categories but do not exceed or fall behind the range spanned by our three focus systems. Notably, none of the investigated species performs best in all four categories. The combination of the performance in each category has direct impact on the resulting solar cell behavior, including optimum thickness and attainable efficiency. The proposed methodology is not limited to VTE OSCs and we expect it to be highly valuable for the solution-processed OSC community to assess the merits of a certain molecule or a combination of donor and acceptor molecule and thereby support the development of novel and better molecules.

Looking forward, there are no fundamental reasons that rule out the possibility of synthesizing VTE donor molecules that combine DCV5T-Me's high extinction with F_4ZnPc's moderate band gap and moderate mobility in the bulk heterojunction, which would already lead to significant improvements in PCE well beyond 10%. Finding evaporable NFAs bears huge potential for achieving not only moderate but low radiative losses for VTE OSCs, as has been the case for solution-processed OSCs. Similarly, the field of VTE OSCs should target higher mobilities in the bulk heterojunction to increase performance, which

might be achieved by tuning the blend morphology via the kinetics during thermal evaporation and/or through designing novel molecules. Conquering this route forward, it should be possible for VTE OSCs to catch up again with the performance of their solution-processed counterparts.

8. Experimental Section

Sample Fabrication: ITO (20 Ohms/sq on Eagle XG glass, rms roughness <7 Å) was purchased from Thin Film Devices TFD Inc., USA. C_{60} was purchased from Creaphys GmbH, Germany, in its optoelectronic grade (sublimed multiple times). ZnPc, F_4ZnPc, DTDCPB, HB194, and BPhen were purchased in a sublimed grade from Luminescence Technology Corp., as well as MoO_3. DCV5T-Me(3,3) was purchased from Synthon Chemicals GmbH & Co. KG, Germany. Prior to deposition, all substrates were cleaned for 10 min in an ultrasonic bath of 2.5% Hellmanex solution, followed by DI water, acetone, and isopropanol. The substrates were treated with O_2 plasma for 10 min before being loaded into the vacuum chamber. All layers were thermally evaporated in a vacuum chamber (EVAP300, Creaphys, base pressure 10^{-7} mbar), followed by transfer into an N_2-filled glovebox without vacuum break for encapsulation. Layers with nominal thickness determined from tooled Quartz Crystal Microbalances were MoOx (3 nm, 0.1 Å s^{-1}), donor:acceptor (2:1 mol., 0.4 Å s^{-1} total rate), BPhen (8 nm, 0.1 Å s^{-1}), Al (≈100 nm, 1 Å s^{-1}). DTDCPB:C_{60} and HB194:C_{60} were evaporated in a 1:1.5 and 1.2:1 molar ratio, respectively, to match high-performing literature reports.[18,20] The solar cells had an active area of 0.08 cm^2 defined by overlapping electrodes and there were eight solar cells per substrate.

Spectroscopic Ellipsometry: SE was carried out with a Woollam RC2 spectroscopic ellipsometer at 55°, 65°, and 75° angles of incidence. Single-component films on glass were prepared in a similar fashion to the devices. The acquired ψ and Δ spectra were model fitted with the CompleteEASE software from J.A. Woollam company to obtain the optical constant n and κ. Anisotropic fits were performed yielding in-plane and out-of-plane components and the results were confirmed by matching transmission data.

Current Density–Voltage: Current density–voltage characteristics were measured under illumination from a Newport Oriel Sol3A solar simulator with a Xe arc lamp. The listed values for J_{sc} and PCE were after spectral mismatch correction[28] carried out post measurement and included an intensity correction to 100 mW cm^{-2} equivalent.

External Quantum Efficiency: Sensitive EQE was measured with a home-built setup based on a Princeton Instrument Spectra Pro monochromator and a Zürich Instruments HF2LI Lock-In amplifier and pre-amplifiers. Optical long pass filters (Thorlabs) were used to enhance sensitivity in the weak absorption regime.

OTRACE: Open-circuit corrected charge carrier extraction was performed with a PAIOS system from Fluxim AG, Switzerland. The samples were illuminated with a white LED light for 100 µs until a steady-state V_{oc} was reached. Delay times were varied between a few µs and 1 ms. The linear voltage pulse (ramp rate between 40 and 50 V ms^{-1} as indicated in the figures) was chosen long enough (between 50 and 80 µs) such that all mobile carriers were extracted, and the current peak decayed to the displacement current obtained from a dark measurement with no offset voltage applied.

Transfer Matrix Method: TMM optical simulations to calculate the short-circuit current density in the case of complete carrier collection (100% IQE) were performed with code published with ref. [60]. A stack of glass, 110 nm of ITO, 3 nm of MoO_3, varied thickness of donor:C_{60}, 8 nm of BPhen, and 100 nm of Al was used with normal incidence of AM1.5g illumination. The complex refractive index $\tilde{n} = n + i\kappa$ of ZnPc, DCV5T-Me, C_{60}, and BPhen were measured in-house with ellipsometry as described above. The $\tilde{n}$ of the blend layer was roughly estimated by linear superposition of the donor and acceptor spectra according to the 2:1 blend ratio. Since the optical simulations were for qualitative purposes only, this approximation was justified. The $\tilde{n}$ of ITO, MoO_3, and Al were taken from ref. [60].

Charge Transfer State Fitting: EQE spectra were fit with Marcus theory $EQE(E) = f_{osc}/(E\sqrt{4\lambda k_B T}) \times \exp(-(E_{CT} + \lambda - E)^2/4\lambda k_B T)$, with CT state energy E_{CT}, reorganization energy λ, and oscillator strength f_{osc}. For ZnPc:C_{60} and F_4ZnPc:C_{60}, the CT state was fitted directly. For DCV5T-Me:C_{60}, the singlet state S1 was fitted first, and then the CT state was fitted to the low-energy region of the difference between the data and the S1 fit.[33,34]

Voltage Loss Calculation: The optical band gap E_g was defined as the inflection point of the EQE absorption edge[12] (on a linear scale, see Figure S2, Supporting Information). Detailed balance theory yields V_{oc}^{SQ} and J_{sc}^{SQ}. The losses from imperfect photocurrent were calculated as $\Delta V_{oc}^{Jsc} = k_B T/q \cdot \ln(J_{sc}^{SQ}/J_{sc})$. The radiative V_{oc}^{rad} was calculated assuming reciprocity between EQE and electroluminescence[36,38] via $V_{oc}^{rad} = k_B T/q \cdot \ln(\int_{E_{min}}^{\infty} EQE \cdot \phi_{AM1.5g}\, dE / \int_{E_{min}}^{\infty} EQE \cdot \phi_{bb}\, dE)$. Here, ϕ_{bb} was the black-body spectrum and E_{min} was chosen small enough such that $V_{oc}^{rad}(E_{min})$ saturates as discussed in Figure S5, Supporting Information. The remaining loss terms were then calculated via $\Delta V_{oc}^{SQ} = E_g - V_{oc}^{SQ}$, $\Delta V_{oc}^{rad} = V_{oc}^{SQ} - \Delta V_{oc}^{sc} - V_{oc}^{rad}$, and $\Delta V_{oc}^{nr} = V_{oc}^{rad} - V_{oc}$. Finally, the LED quantum efficiency was obtained from $\Delta V_{oc}^{nr} = k_B T/q \cdot \ln(Q_{LED}^{-1})$.

Supporting Information

Supporting Information is available from the Wiley Online Library or from the author.

Acknowledgements

P.K. and M.K.R. acknowledge funding from the Global Challenges Research Fund (GCRF) through Science & Technology Facilities Council (STFC), grant number ST/R002754/1: Synchrotron Techniques for African Research and Technology (START). A.J. acknowledges funding from the Department of Physics at the University of Oxford and a Wolfson-Marriott Scholarship by Wolfson College. I.H. acknowledges funding from the Oppenheimer Memorial Trust and the FirstRand Foundation. S.V.K. expresses his gratitude to EPSRC (WAFT, Grants No. EP/M015173/1; IAA and No. EP/R511742/1) for funding. M.N. acknowledges funding from the Academy of Finland through project # 326000.

Conflict of Interest

The authors declare no conflict of interest.

Author Contributions

The original draft of the paper was written by PK with all authors contributing to reviewing and editing. PK prepared, measured, and lead the analysis of the samples with the exception of ellipsometry, which was measured and analysed by IH and SVK. AJ performed the CT fits. MN advised on the charge transport measurements and analysis. The project was conceived by PK and MKR. MKR supervised the project.

Data Availability Statement

The data that support the findings of this study are available from the corresponding author upon reasonable request.

Keywords

mobility, organic solar cells, small molecules, transport and recombination, vacuum thermal evaporation, voltage loss

Received: September 22, 2021
Revised: November 18, 2021
Published online: December 19, 2021

[1] Y. Cui, Y. Xu, H. Yao, P. Bi, L. Hong, J. Zhang, Y. Zu, T. Zhang, J. Qin, J. Ren, Z. Chen, C. He, X. Hao, Z. Wei, J. Hou, *Adv. Mater.* **2021**, *33*, 2102420.
[2] M. Riede, D. Spoltore, K. Leo, *Adv. Energy Mater.* **2021**, *11*, 2002653.
[3] Y. Huo, H. L. Zhang, X. Zhan, *ACS Energy Lett.* **2019**, *4*, 1241.
[4] P. Meredith, A. Armin, *Nat. Commun.* **2018**, *9*, 5261.
[5] M. Nyman, O. J. Sandberg, W. Li, S. Zeiske, R. Kerremans, P. Meredith, A. Armin, *Sol. RRL* **2021**, *5*, 2100018.
[6] X. Che, C. L. Chung, C. C. Hsu, F. Liu, K. T. Wong, S. R. Forrest, *Adv. Energy Mater.* **2018**, *8*, 1703603.
[7] J. Zhao, Y. Li, G. Yang, K. Jiang, H. Lin, H. Ade, W. Ma, H. Yan, *Nat. Energy* **2016**, *1*, 15027.
[8] V. Vohra, K. Kawashima, T. Kakara, T. Koganezawa, I. Osaka, K. Takimiya, H. Murata, *Nat. Photonics* **2015**, *9*, 403.
[9] Q. Burlingame, X. Huang, X. Liu, C. Jeong, C. Coburn, S. R. Forrest, *Nature* **2019**, *573*, 394.
[10] J. Benduhn, K. Tvingstedt, F. Piersimoni, S. Ullbrich, Y. Fan, M. Tropiano, K. A. McGarry, O. Zeika, M. K. Riede, C. J. Douglas, S. Barlow, S. R. Marder, D. Neher, D. Spoltore, K. Vandewal, *Nat. Energy* **2017**, *2*, 17053.
[11] M. C. Scharber, D. Mühlbacher, M. Koppe, P. Denk, C. Waldauf, A. J. Heeger, C. J. Brabec, *Adv. Mater.* **2006**, *18*, 789.
[12] U. Rau, B. Blank, T. C. M. Müller, T. Kirchartz, *Phys. Rev. Appl.* **2017**, *7*, 044016.
[13] P. Kaienburg, U. Rau, T. Kirchartz, *Phys. Rev. Appl.* **2016**, *6*, 24001.
[14] R. Fitzner, E. Mena-Osteritz, A. Mishra, G. Schulz, E. Reinold, M. Weil, C. Körner, H. Ziehlke, C. Elschner, K. Leo, M. Riede, M. Pfeiffer, C. Uhrich, P. Bäuerle, *J. Am. Chem. Soc.* **2012**, *134*, 11064.
[15] J. Meiss, A. Merten, M. Hein, C. Schuenemann, S. Schäfer, M. Tietze, C. Uhrich, M. Pfeiffer, K. Leo, M. Riede, *Adv. Funct. Mater.* **2012**, *22*, 405.
[16] F. Yang, K. Sun, S. R. Forrest, *Adv. Mater.* **2007**, *19*, 4166.
[17] D. Wynands, M. Levichkova, K. Leo, C. Uhrich, G. Schwartz, D. Hildebrandt, M. Pfeiffer, M. Riede, *Appl. Phys. Lett.* **2010**, *97*, 073503.
[18] Y. Zou, J. Holst, Y. Zhang, R. J. Holmes, *J. Mater. Chem. A* **2014**, *2*, 12397.
[19] X. Xiao, K. J. Bergemann, J. D. Zimmerman, K. Lee, S. R. Forrest, *Adv. Energy Mater.* **2014**, *4*, 1301557.
[20] V. Steinmann, N. M. Kronenberg, M. R. Lenze, S. M. Graf, D. Hertel, K. Meerholz, H. Bürckstümmer, E. v. Tulyakova, F. Würthner, *Adv. Energy Mater.* **2011**, *1*, 888.
[21] M. Zhang, H. Wang, H. Tian, Y. Geng, C. W. Tang, *Adv. Mater.* **2011**, *23*, 4960.
[22] R. Pandey, Y. Zou, R. J. Holmes, *Appl. Phys. Lett.* **2012**, *101*, 033308.
[23] H. W. Lin, L. Y. Lin, Y. H. Chen, C. W. Chen, Y. T. Lin, S. W. Chiu, K. T. Wong, *Chem. Commun.* **2011**, *47*, 7872.
[24] T. Kirchartz, P. Kaienburg, D. Baran, *J. Phys. Chem. C* **2018**, *122*, 5829.
[25] P. Kaienburg, L. Krückemeier, D. Lübke, J. Nelson, U. Rau, T. Kirchartz, *Phys. Rev. Res.* **2020**, *2*, 023109.
[26] M. S. Vezie, S. Few, I. Meager, G. Pieridou, B. Dörling, R. S. Ashraf, A. R. Goñi, H. Bronstein, I. McCulloch, S. C. Hayes, M. Campoy-Quiles, J. Nelson, *Nat. Mater.* **2016**, *15*, 746.
[27] A. Armin, W. Li, O. J. Sandberg, Z. Xiao, L. Ding, J. Nelson, D. Neher, K. Vandewal, S. Shoaee, T. Wang, H. Ade, T. Heumüller, C. Brabec, P. Meredith, *Adv. Energy Mater.* **2021**, *11*, 2003570.
[28] V. Shrotriya, G. Li, Y. Yao, T. Moriarty, K. Emery, Y. Yang, *Adv. Funct. Mater.* **2006**, *16*, 2016.
[29] D. Bartesaghi, I. del Carmen Pérez, J. Kniepert, S. Roland, M. Turbiez, D. Neher, L. J. A. Koster, *Nat. Commun.* **2015**, *6*, 7083.
[30] R. S. Crandall, *J. Appl. Phys.* **1982**, *53*, 3350.
[31] C. Falkenberg, K. Leo, M. K. Riede, *J. Appl. Phys.* **2011**, *110*, 124509.
[32] R. Meerheim, C. Körner, K. Leo, *Appl. Phys. Lett.* **2014**, *105*, 063306.
[33] V. C. Nikolis, Y. Dong, J. Kublitski, J. Benduhn, X. Zheng, C. Huang, A. C. Yüzer, M. Ince, D. Spoltore, J. R. Durrant, A. A. Bakulin, K. Vandewal, *Adv. Energy Mater.* **2020**, *10*, 2002124.
[34] T. Li, J. Benduhn, Y. Li, F. Jaiser, D. Spoltore, O. Zeika, Z. Ma, D. Neher, K. Vandewal, K. Leo, *J. Mater. Chem. A* **2018**, *6*, 18583.
[35] T. Moench, P. Friederich, F. Holzmueller, B. Rutkowski, J. Benduhn, T. Strunk, C. Koerner, K. Vandewal, A. Czyrska-Filemonowicz, W. Wenzel, K. Leo, *Adv. Energy Mater.* **2016**, *6*, 1501280.
[36] U. Rau, *Phys. Rev. B* **2007**, *76*, 085303.
[37] K. Vandewal, K. Tvingstedt, A. Gadisa, O. Inganäs, J. v. Manca, *Nat. Mater.* **2009**, *8*, 904.
[38] W. Shockley, H. J. Queisser, *J. Appl. Phys.* **1961**, *32*, 510.
[39] J. Yao, T. Kirchartz, M. S. Vezie, M. A. Faist, W. Gong, Z. He, H. Wu, J. Troughton, T. Watson, D. Bryant, J. Nelson, *Phys. Rev. Appl.* **2015**, *4*, 014020.
[40] Y. Wang, D. Qian, Y. Cui, H. Zhang, J. Hou, K. Vandewal, T. Kirchartz, F. Gao, *Adv. Energy Mater.* **2018**, *8*, 1801352.
[41] M. Azzouzi, T. Kirchartz, J. Nelson, *Trends Chem.* **2019**, *1*, 49.
[42] X.-K. Chen, D. Qian, Y. Wang, T. Kirchartz, W. Tress, H. Yao, J. Yuan, M. Hülsbeck, M. Zhang, Y. Zou, Y. Sun, Y. Li, J. Hou, O. Inganäs, V. Coropceanu, J.-L. Bredas, F. Gao, *Nat. Energy* **2021**, *6*, 799.
[43] A. Baumann, J. Lorrmann, D. Rauh, C. Deibel, V. Dyakonov, *Adv. Mater.* **2012**, *24*, 4381.
[44] G. Juška, K. Arlauskas, M. Viliūnas, J. Kočka, *Phys. Rev. Lett.* **2000**, *84*, 4946.
[45] J. A. Röhr, T. Kirchartz, J. Nelson, *J. Phys.: Condens. Matter* **2017**, *29*, 205901.
[46] J. A. Röhr, D. Moia, S. A. Haque, T. Kirchartz, J. Nelson, *J. Phys.: Condens. Matter* **2018**, *30*, 105901.
[47] O. J. Sandberg, M. Nyman, *Org. Electron.* **2019**, *64*, 97.
[48] G. Juška, K. Arlauskas, M. Viliūnas, J. Kočka, *Phys. Rev. Lett.* **2000**, *84*, 4946.
[49] J. Lorrmann, B. H. Badada, O. Inganäs, V. Dyakonov, C. Deibel, *J. Appl. Phys.* **2010**, *108*, 113705.
[50] O. J. Sandberg, M. Nyman, S. Dahlström, S. Sandén, B. Törngren, J. H. Smått, R. Österbacka, *Appl. Phys. Lett.* **2017**, *110*, 153504.
[51] D. Kiermasch, A. Baumann, M. Fischer, V. Dyakonov, K. Tvingstedt, *Energy Environ. Sci.* **2018**, *11*, 629.
[52] M. Azzouzi, P. Calado, A. M. Telford, F. Eisner, X. Hou, T. Kirchartz, P. R. F. Barnes, J. Nelson, *Sol. RRL* **2020**, *4*, 1900581.
[53] T. Kirchartz, J. Nelson, *Phys. Rev. B* **2012**, *86*, 165201.
[54] S. H. Park, A. Roy, S. Beaupré, S. Cho, N. Coates, J. S. Moon, D. Moses, M. Leclerc, K. Lee, A. J. Heeger, *Nat. Photonics* **2009**, *3*, 297.
[55] F. D. Eisner, M. Azzouzi, Z. Fei, X. Hou, T. D. Anthopoulos, T. J. S. Dennis, M. Heeney, J. Nelson, *J. Am. Chem. Soc.* **2019**, *141*, 6362.
[56] M. Azzouzi, J. Yan, T. Kirchartz, K. Liu, J. Wang, H. Wu, J. Nelson, *Phys. Rev. X* **2018**, *8*, 031055.
[57] X. K. Chen, V. Coropceanu, J. L. Brédas, *Nat. Commun.* **2018**, *9*, 5295.
[58] M. Katayama, T. Kaji, S. Nakao, M. Hiramoto, *Front. Energy Res.* **2020**, *8*, 4.
[59] S. Dahlström, C. Ahläng, K. Björkström, S. Forsblom, B. Granroth, K. Jansson, A. Luukkonen, M. T. Masood, J. Poulizac, S. Qudsia, M. Nyman, *AIP Adv.* **2020**, *10*, 065203.
[60] G. F. Burkhard, E. T. Hoke, M. D. McGehee, *Adv. Mater.* **2010**, *22*, 3293.